Evaluation of the thermal phonon emission in dynamic fracture of brittle crystals

Fouad Atrash and Dov Sherman*
Department of Materials Engineering, Technion, Haifa-32000, Israel
(Received 22 September 2011; revised manuscript received 4 December 2011; published 21 December 2011)

We describe in detail how to quantify, computationally, the contribution of the anisotropic and velocity-dependent thermal phonon emission energy release rate during dynamic crack propagation in brittle crystals. The calculations were performed using a procedure based on combined continuum elastodynamics Freund equation of motion and molecular dynamics computer calculations. We used a precracked strip-like specimen subjected to prescribed displacement on the boundaries, commonly used in atomistic calculations of crack dynamics. Various cleavage planes and directions of silicon-like crystal for a wide range of crack speeds were investigated. It is shown that in addition to being strongly dependant on crack speed and atomistic arrangement, the relative phonon emission energy release rate is size dependent, hence governing the size-dependent terminal crack speed. This speed, however, is not influenced by the specimen's initial temperature, ranging between 10K and 300K.

DOI: 10.1103/PhysRevB.84.224307 PACS number(s): 62.20.mj, 46.50.+a, 02.70.Ns, 63.20.dd

I. INTRODUCTION

Dynamic fracture of brittle crystals is a ubiquitous problem, with several fundamental questions still remaining of broad interest for various engineering and scientific communities that have to be resolved. For example, continuum mechanics defined the Rayleigh free surface waves speed, C_R, as the upper limit for crack propagation under tensile stresses,[1,2] butthe fastest crack speed measured experimentally in silicon crystal ranges between 0.7 and $0.9C_R$. Fracture surface and crack path instabilities on several length scales observed recently in silicon are other key phenomena that cannot be resolved with the existing theories of dynamic fracture and require thorough explanations.

During recent decades, a huge effort was invested on exploring the fracture process from the atomistic scale, and the dynamics of crack propagation has been analyzed by computer calculations with atomistic resolution. The classical theory of dynamic fracture[1] is based on continuum isotropic elastodynamics; thus, it cannot account for phenomena emerging from the discrete atomistic nature of the fracture processes, among them, thermal phonon emission, or heat, generated during rapid crack propagation. The temperature rise in the vicinity of a crack tip may be large enough to influence the energy balance, fracture features, and path. Thus, a precise treatment of heat distribution during crack propagation is required.

In metals, the crack propagation process involves heat generation. A temperature rise of 130K was measured at a distance of 30 μm from crack propagation in pure Fe, and higher temperatures were expected to exist at the crack tip. The energy associated with the thermal radiation was approximately 90% of the irreversibly consumed energy.[3] The formation of a crazed zone at the tip of glassy polymers results in the evolution of heat along the crack path. A temperature rise of about 500K was measured at a distance of 0.5 mm from the path of crack propagation in poly(methyl methacrylate) (PMMA), and the energy associated with the thermal radiation was approximately 60%–80% of the irreversibly consumed energy,[4] A temperature rise of about 0.0015K was measured at a distance of 2.5 mm from a crack propagating in brittle isotropic materials; thermal models that treat the crack as a heat-generating source were used to estimate the temperature rise at the crack tip. Significant temperature elevations at the crack tip were estimated (3200K in glass[5] and 4700K in quartz[6]).

Attempts have been made to create theoretical formulations to predict this temperature rise. The suggested theoretical models may be divided into two categories: models which did not take into account the coupling between the thermal and the mechanical fields in the vicinity of the crack tip[4–8] and models that attempted to extend the fracture mechanics models by suggesting a new approach that coupled the thermal and mechanical fields in the vicinity of the crack tip.[9–12]

Several authors have suggested that heat or thermal phonon emission energy may play a significant role in the dynamics of brittle fracture in crystals. Hauch and others[13,14] performed dynamic fracture experiments in silicon-like brittle crystal; they noticed that crack dynamics dissipated more than seven times the energy needed to create flat surfaces. Their molecular dynamic (MD) calculations, using a modified Stillinger–Weber interatomic potential, indicated that the extra energy is dissipated by lattice vibrations. Gumbsch *et al.*[15] performed MD calculations of dynamic fracture in two-dimensional (2D) triangular brittle crystal, using the Morse potential. They suggested that phonon emission prohibits the crack from attaining the Rayleigh surface wave speed, C_R. Sherman and coworkers[16–19] performed three-point bending cleavage experiments in silicon. Their results indicated that cleavage energy increased anisotropically with crack speed; this may be responsible for crack deflection from the (110) plane into the (111) plane due to anisotropic phonon emission. Swadener *et al.*[20] performed MD simulation of dynamic fracture in silicon, using the modified embedded atom method (MEAM) potential. Their MD results indicated that the phonon emission energy (elastic and thermal) is approximately equal to the energy dissipated by the elastic waves, as predicted by the continuum theory of linear fracture. It is noted that Swadener *et al.* have performed dynamic fracture in highly strained samples; the atoms in the crack tip vicinity were highly disturbed from their equilibrium, and the cracked surface included surface instabilities and plastic deformation. This behavior contradicts experimental results that show atomically flat surfaces even in highly strained specimens.[21]

We suggest that the missing link to resolve several fundamental queries in dynamic fracture in brittle single crystals is hidden in the anisotropic, velocity-dependent lattice vibrations or thermal phonons emitted from the crack tip during the fracture dynamics. The current contribution, therefore, aims at a thorough description of the calculations of the phonon emission energy release rate (ERR), $\mathcal{G}_{\rm ph}$, generated during dynamic crack propagation in brittle crystals by MD computer calculations. Such calculations will help to better understand the origin of surface instabilities and crack path instability and to resolve the question of why the crack terminal velocity is lower than the theoretical limit.

II. THEORY

The material response (crack speed) to the driving force (strain ERR) during dynamic crack propagation in an isotropic infinite plate made of brittle material under Mode I loading was described by the Freund equation of motion.[1] It was suggested that the formalism for $\mathcal{G}$, the net energy available for the bond-breaking mechanisms, can be approximated by a product of a linear function of the crack speed, V, and the applied quasi-static strain ERR, $\mathcal{G}_0$:

$$\mathcal{G}_{\rm ph} = \mathcal{G}_0\,(1 - V/C_{\rm R}) = 2\gamma_s, \tag{1}$$

where $2\gamma_s$ is twice the surface energy of the material.

The physical interpretation of Eq. (1) is that when applying $\mathcal{G}_0$ greater than the energy required for bond breaking, $2\gamma_s$, the excess energy is converted into kinetic energy. We postulate that with this rational, $\mathcal{G}$ and $\mathcal{G}_0$ are appropriate for isotropic as well as anisotropic materials. Furthermore, we interpret Eq. (1) as follows: $\mathcal{G} = \mathcal{G}_0 - \mathcal{G}_0(V/C_{\rm R}) = \mathcal{G}_0 - \mathcal{G}_{\rm K}$, where $\mathcal{G}_{\rm K}$ is the kinetic energy of the *elastic waves* defined by Freund, hence:

$$\mathcal{G}_{\rm K}^{\rm F} = \mathcal{G}_0 - 2\gamma_s = \mathcal{G}_0\frac{V}{C_{\rm R}} \tag{2}$$

We further define the elastic waves ERR, $\mathcal{G}_{\rm K}^{\rm F}$, as an explicit function of the crack speed by substituting Eq. (1) into Eq. (2)

$$\frac{\mathcal{G}_{\rm K}^{\rm F}}{2\gamma_s} = \frac{V/C_{\rm R}}{1 - V/C_{\rm R}} \tag{3}$$

It is noted that the energy available for the bond breaking mechanisms, $\mathcal{G}$, Eq. (1), is defined by the continuum based elastodynamic equations using Rice J-Integral:

$$\mathcal{G} = \lim_{\Gamma\to 0}\left\{\frac{1}{V}\int_{\Gamma}\left[\sigma_{ij}n_j\frac{\partial u_i}{\partial t} + (U+T)\,V n_1\right]d\Gamma\right\} \tag{4}$$

where,

$$U = \int_{x_1 - Vt}^{\infty}\sigma_{ji}\frac{\partial^2 u_i}{\partial x_j\partial\xi}d\xi\,,\quad T = \frac{1}{2}\rho V^2\frac{\partial u_i}{\partial x_1}\frac{\partial u_i}{\partial x_1} \tag{5}$$

To understand the nature of the kinetic ERR, $\mathcal{G}_{\rm K}^{\rm F}$, remember that the dynamic counterpart of the strain ERR, which is called the dynamic ERR, contains the term T in Eq. (5), which is the kinetic energy added to the body due to crack motion. This addition is proportional to V^2 and thus takes into account only the phenomena that contribute to the total linear momentum of the cracked body; the term T assumes that the kinetic energy is stored only in the form of elastic waves. Thus, the Freund equation of motion is unable to capture any thermal vibrations that do not affect the total linear momentum of the cracked body. Unlike continuum mechanics, MD can capture the atomistic events at the crack tip and thus take into account the effects of the energy dissipated by phonon emission. This energy is expected to cause a deviation from the Freund equation of motion. Therefore, we suggest the definition of a new kinetic ERR term, $\mathcal{G}_{\rm K}^{\rm MD}$, that takes into account the change in kinetic energy due to elastic waves and includes thermal phonon emission generated during crack dynamics. This term can be evaluated using:

$$\mathcal{G}_{\rm K}^{\rm MD} = 2\frac{\partial E_{\rm Kinetic}}{\partial A} \tag{6}$$

where $E_{\rm Kinetic}$ is the instantaneous total kinetic energy of the cracked body. The factor 2 originates from the equipartition theory (i.e., waves emitted from the crack tip carry equal amounts of average potential energy and kinetic energy).

For cracks propagating at constant speed, V, Eq. (6) takes the following form,

$$\mathcal{G}_{\rm K}^{\rm MD} = 2\frac{\partial E_{\rm Kinetic}}{\partial(aBt)} = \frac{2}{BV}\frac{\partial E_{\rm Kinetic}}{\partial t} \tag{7}$$

where a is the crack length, and B is the width of the specimen. Similar methodology for calculating $\mathcal{G}_{\rm K}^{\rm MD}$ was used by Jin *et. al.*[22] for dislocation dynamics.

The instantaneous total kinetic energy, $E_{\rm Kinetic}$, of the system was calculated based on the instantaneous velocities of the atoms as follows:

$$E_{\rm Kinetic} = \sum_{i=1}^{N}\frac{m}{2}\left(v_x^2 + v_y^2 + v_z^2\right), \tag{8}$$

where N is the number of atoms in the system, m is the mass of the atom, and v_α is the velocity of atom i in the α direction. The suggested kinetic ERR, $\mathcal{G}_{\rm K}^{\rm MD}$, contains contributions of the elastic wave ERR and the thermal phonon emission ERR, termed $\mathcal{G}_{\rm ph}$; thus,

$$\frac{\mathcal{G}_{\rm ph}}{2\gamma_s} = \frac{\mathcal{G}_{\rm K}^{\rm MD}}{2\gamma_s} - \frac{\mathcal{G}_{\rm K}^{F}}{2\gamma_s} = \frac{\mathcal{G}_{\rm K}^{\rm MD}}{2\gamma_s} - \frac{(V/C_{\rm R})}{1-(V/C_{\rm R})} \tag{9}$$

It is noted that the elastic constants vary along the crack propagation direction; therefore, $C_{\rm R}$ is not a direct function of the strains. Hence, we chose to use $C_{\rm R}$ of the relaxed crystal. We used Eq. (9) to calculate the phonon emission ERR. A graphical representation of Eq. (9) is shown in Fig. 1.

III. THE COMPUTATIONAL METHOD

The research of dynamic fracture by atomistic calculations is still in its first steps; this fact is clear when comparing the different loading schemes, boundary conditions, and specimen geometry that were used by different researchers. The choice of the details of the computer experiments is critical and may affect the results and their interpretation. In this study we decided to follow the computational scheme suggested by Gumbsch *et al.*,[15] and to adjust it to meet our purposes.

The computer "experiments" in this study were performed by utilizing the ITAP-IMD MD code.[23] This is a C program that can handle both parallel MD calculations and molecular statics

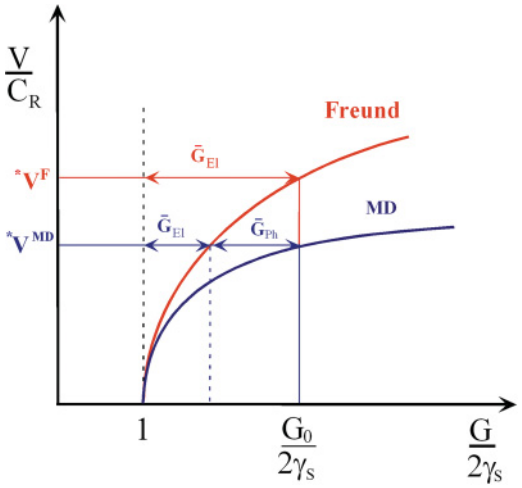

FIG. 1. (Color online) Schematic presentation of the normalized crack speed vs the normalized strain ERR by the Freund equation of motion (red/dark gray line) and MD calculations (blue/medium gray line); the difference is attributed to the energy dissipated by phonon emission ERR, $\mathcal{G}_{\rm ph}$. Star denotes normalization by $C_{\rm R}$, bar by $2\gamma_s$.

calculations. The Technion RBNI NANCO computer cluster was used to perform most of the calculations in this study. This cluster comprises 64 nodes, each with four dual-core AMD Opteron 1.8-GHz CPU units. We used the modified Stillinger–Weber (SW) potential[14,24] to describe a *model* of a brittle crystal with a diamond structure unit cell with lattice parameter 5.431 Å.

The "experiment" can be divided into five stages, schematically shown in Fig. 2: (i) sample preparation, (ii) quasi-static loading, (iii) MD crack initiation, (iv) homogeneous rescaling, and (v) MD crack propagation, which is described in this section. The computational data obtained at the crack propagation stage, which was used to calculate the phonon ERR, is described in the next section.

A. Specimen preparation

In this investigation, we used a strip-like specimen commonly used in atomistic calculations of dynamic fracture: a

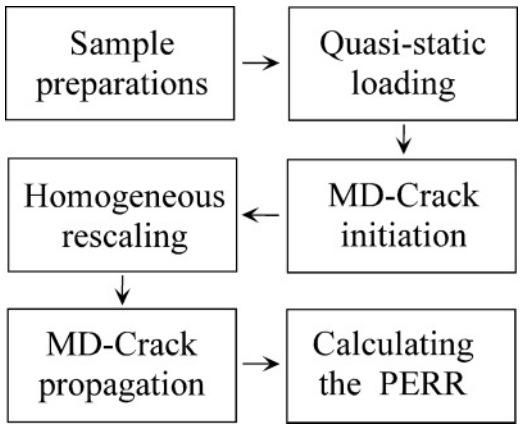

FIG. 2. Flowchart of the dynamic fracture computer "experiments" performed in this study.

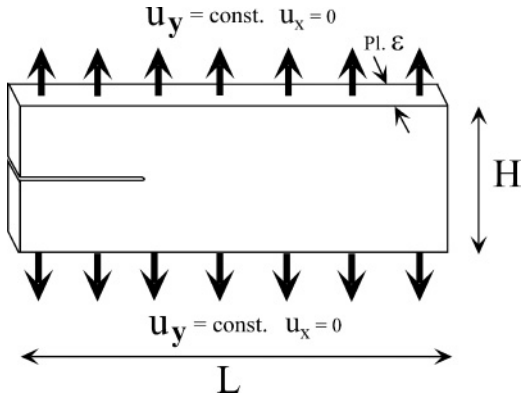

FIG. 3. A schematic presentation of the strip-like specimen dimensions and boundary conditions.

long specimen containing a crack, subjected to constant tensile displacement on the boundaries parallel to the crack surfaces, as shown in Fig. 3. Periodic boundary conditions were used along the crack front direction. This specimen geometry allows for crack propagation under constant driving force, $\mathcal{G}_0$, and thus at a constant crack speed, V, which is achieved immediately after propagation. The quasi-static strain ERR of this specimen is given by:[25]

$$\mathcal{G}_0 = \tfrac{1}{2} \cdot H \cdot E^* \varepsilon_{yy}^2, \tag{10}$$

where $\varepsilon_{yy} = u_y/H$ is the remote applied strain normal to the crack surface direction, which is correlated to a fixed displacement, u_y, of the boundaries, and H is the height of the specimen. E^* is the effective elastic modulus. It is clear from Eq. (10) that the strain ERR does not depend on the crack length. Thus, the crack speed can be tuned by applying different values of u_y. It is noted that the effective secular elastic constant E^* in Eq. (10) is determined in separate calculations using the modified SW interatomic potential; E^* varies nearly linearly with ε_{yy}, where $dE^*/d\varepsilon_{yy}$ is approximately 8 GPa for each 1% strain for all the cleavage systems.

The atomistic strip-like specimens were filled with our model material and aligned at different directions on the (111) and (110) low-energy cleavage planes of silicon crystal. We kept the aspect ratio of the specimen, H/L, at 1:3. The dimensions of the specimens were about 450 × 160 × 20 (in Å). Each specimen included about 100,000 atoms. Seven different cleavage systems (planes and directions) were investigated. A precrack, 20% of the length of the specimen (nearly 40 atoms), was created by removing one atomic layer in the middle of the sample's height. The atomic configurations near the crack tip of the initial specimens are visualized in Figs. 4 and 5.

B. Quasi-static loading

To obtain the displacement field of a stable crack at 0K, the specimens were loaded quasi-statically by cycles of homogenous strain (10^{-5}) followed by relaxation using a conjugate gradient (CG) method. At a critical strain level, namely, the lattice trapping limit, the minimal energy of the specimens were that of two relaxed pieces of the model

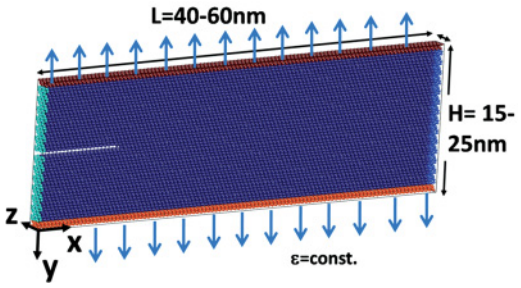

FIG. 4. (Color online) Visualization of the initial atomic configuration.

material. The strained atomic configuration of the (110)[1$\bar{1}$0] cleavage system is visualized in Fig. 6 for example. The lowest lattice trapping strain, $\varepsilon_{yy} = 5.97\%$, was measured in the (110)[1$\bar{1}$2] cleavage system, and the highest, $\varepsilon_{yy} = 7.76\%$, was measured in the (111)[1$\bar{1}$0] cleavage system. According to Eqs. (1) and (10), the minimal strains at propagation for the (110) and (111) planes are 4.8% and 4.4%, respectively.

C. Crack initiation

The computational effect of lattice trapping prohibits simulating crack propagation with classical molecular dynamics at a strain level below the lattice-trapping limit without a trigger, usually, a localize heating of the crack tip.[14,15,20] In this study, we focused on phonon emission and were interested in avoiding any artificial perturbation in the vibrational field. Therefore, a stepwise loading scheme is suggested: that is, crack initiation at a small strain increment below the lattice trapping limit, followed by a gradual homogeneous rescaling of the strain field to the desired strain level. This scheme keeps the spatial distribution of the strain field as that of a stable crack and generates a vibrational field around the crack tip that replaces the artificial thermal trigger used by other researchers.

The atomic configurations of the quasi-statically strained samples one strain increment before the quasi-static fracture occurred were used as an input for microcanonical MD simulation. The initial velocities of the atoms were set to distribute normally around an average speed equivalent to 10K.

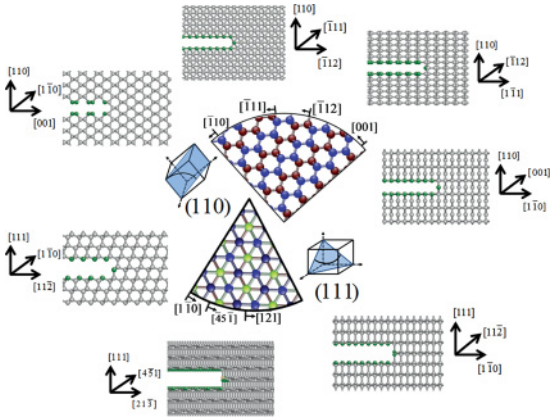

FIG. 5. (Color online) Visualization of the atomic arrangements near the crack tips for seven cleavage systems considered in this study.

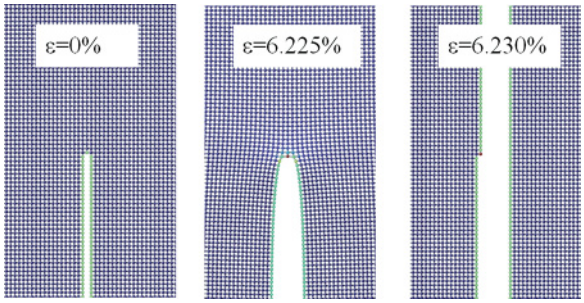

FIG. 6. (Color online) The deformation of the strip-like specimen of the (110)[1$\bar{1}$0] cleavage system: applying an additional strain increment beyond a critical value caused the specimen to split into two relaxed parts. The lattice trapping strain for this case is 6.23%.

The MD simulation integration time step was set to 0.1 fs. Starting from this stage in our computer experiment, fixed boundary conditions to all the outermost two atomic layers were applied.

A microcanonical MD simulation using the ITAP-IMD code was performed. The atomic configuration of the (110)[1$\bar{1}$0] cleavage system is visualized in Fig. 7. It can be seen qualitatively that the fracture propagated in a brittle manner. The atomic instantaneous temperature demonstrated a local temperature rise up to 187K in the vicinity of the crack tip.

D. Specimen rescaling

We stopped the MD simulation after the crack ruptured about 40 bonds, then we reduced the strain gradually and homogeneously to the desired strain. The strain difference between the lattice trapping strain and the desired strain was divided into six or 12 increments, each about 0.1%, and then we reduced the strain each 100 fs by one strain increment. This procedure aimed to reduce the effect of possible shock waves that may emerge from the rescaling action.

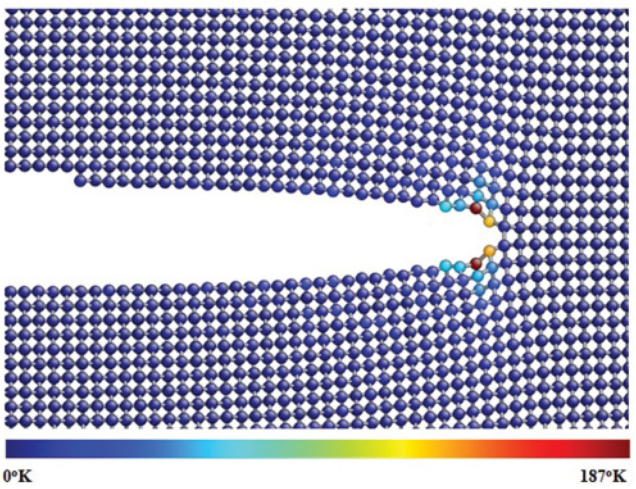

FIG. 7. (Color online) Visualization of the atomic configuration after crack initiation stage. The colors/shades of gray represent instantaneous local temperature.

E. Crack propagation

The rescaled specimens were used as input configurations for another MD simulation, in which the crack is expected to propagate at a constant speed. In this stage, we fixed the two outermost atomic layers along the specimen's perimeter (Fig. 5) to prevent energy dissipation by surface reconstruction or surface waves.

The response of the simulated material to the applied strain in this stage of the simulation can be divided to three regimes:

1. Low strains

Reducing the strain ε_{yy} below a critical value stopped the initially propagating crack. This critical value is higher than the strain needed to create atomically flat, free surfaces. This behavior is called the "velocity gap" effect.[14] For example, on the (111)[11$\bar{2}$], (111)[1$\bar{1}$0], and (111)[$\bar{2}$13] cleavage systems, no crack propagation was possible for $\varepsilon_{yy} < 6.9\%$, 5.6%, and 5.1%, respectively, where the energy needed to create atomically flat, free surfaces is equivalent to applying $\varepsilon_{yy} = 4.2\%$. Note that these strain values change with sample height, as shown by Eq. (10).

2. Intermediate strains

We successfully simulated atomically flat brittle dynamic crack propagation by decreasing or increasing the strain ε_{yy} from the lattice-trapping strain. The brittle behavior was achieved for the relatively wide strain interval. For example, on the (110)[1$\bar{1}$0] cleavage system, brittle crack propagation was achieved for the range $\varepsilon_{yy} = 4.7\%$–9.6%.

3. High strains

Increasing the strain ε_{yy} beyond a critical value yielded surface instabilities, dislocations, and atomic-size cagelike structures in the vicinity of the crack tip, as shown in Fig. 8. We attribute this behavior to the inability of the SW interatomic potential to describe the accurate material behavior at high strains. Moreover, shock waves emanated from the crack tip at this strain level and helped to distort the atomic arrangement from the crystalline state.

We excluded from our results crack dynamics on the (110)[001] cleavage system. In this system, crack propagation on the (110) cleavage plane was almost impossible; the crack was immediately deflected to the (111)[11$\bar{2}$] cleavage system (Fig. 9). This result coincides with a recently published concurrent multiscale simulation[26] that was used to describe the crack deflection phenomenon.

The crack tip position and the kinetic energy were calculated during crack propagation for the first 4 ps of the MD runs to avoid interaction between reflected waves and the crack tip.

IV. RESULTS

A. Evaluating the crack speed

The crack speed was measured based on the crack tip position vs time. The crack tip was located on the basis of an algorithm that combined the identification of the atom that has the maximal potential energy and the maximal displacement normal to the cleavage plane (from the uncracked side). The error in locating the crack position with this procedure is less than one lattice parameter. For example, the crack tip position as a function of time of a crack propagating on the (110)[1$\bar{1}$0] cleavage system is shown in Fig. 10. The crack speed was estimated by a linear best fit procedure of the crack tip vs time plot. The error in the crack speed measurement is about 0.1 km/s.

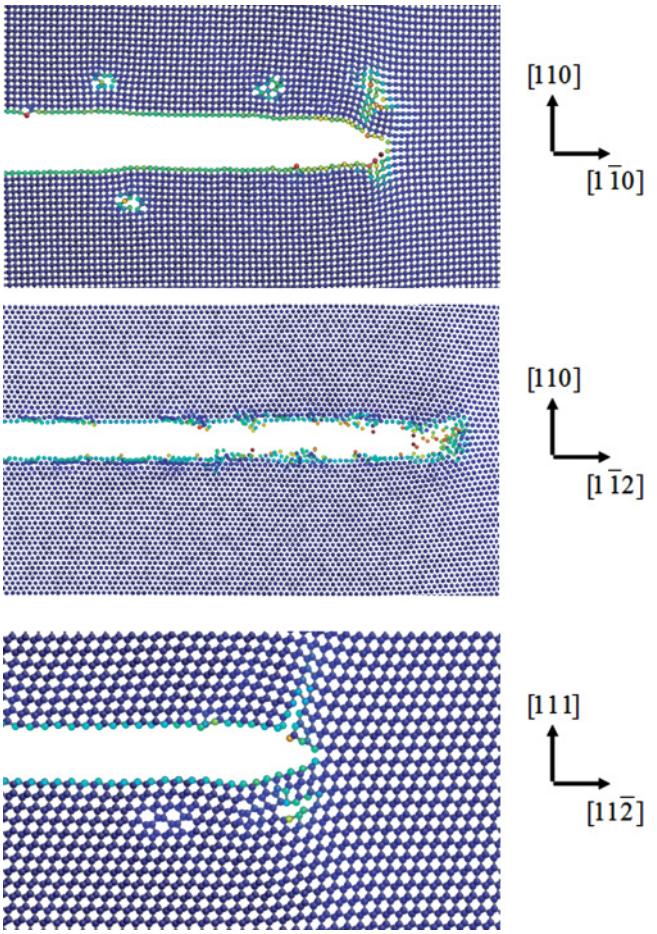

FIG. 8. (Color online) Typical surface instabilities observed in a highly strained specimen.

B. Calculating the kinetic energy

The variation of E_{Kinetic} vs time was recorded during the course of crack propagation. Plot of E_{Kinetic} vs time for different normalized strain ERR for crack propagating on the (110)[1$\bar{1}$0] cleavage system is shown in Fig. 11. It can be seen

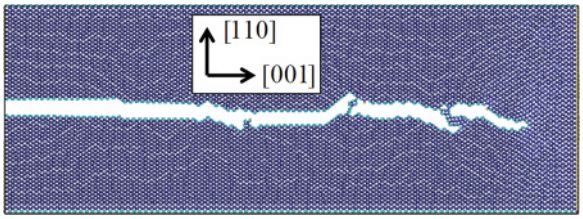

FIG. 9. (Color online) Crack propagation on the (110)[001] cleavage system of silicon is unstable; the crack tends to deflect to the (111)[11$\bar{2}$] cleavage system.

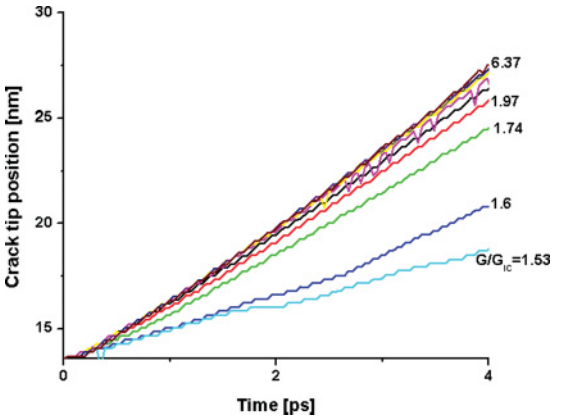

FIG. 10. (Color online) Crack tip position vs time for different strain ERR values of a crack propagating on the (110)[1$\bar{1}$0] cleavage system of a single silicon crystal.

that the variation of E_{Kinetic} with time is approximately linear at low $\mathcal{G}_0$, and increasing wavy fluctuations around the linear trend are evident at high $\mathcal{G}_0$. This wavy pattern is attributed to elastic waves emitted due to elastic fluctuations of the free surfaces during crack dynamics. The fine fluctuations that lie on the wavy structure were attributed to the thermal fluctuation of the atoms due to the initial temperature and the thermal phonons emitted by the crack tip motion.

C. Energy-speed relationships

The normalized crack speed vs normalized $\mathcal{G}_0$ for the six cleavage systems is shown in Fig. 12, and the normalized crack speed vs the normalized total kinetic ERR for these systems is shown in Fig. 13.

The stability of the MD calculated total kinetic energy is readily demonstrated (Fig. 13). The prediction of the Freund equation of motion is excellent up to $V/C_{\text{R}} \sim 0.5$; thereafter, the crack speed decreases due to the increased energy consumed by phonon emission. The pronounced anisotropy of the energy-speed relationship is evident in both Fig. 12 and Fig. 13.

The variations of the total kinetic ERR with the strain ERR for the system under investigation were evaluated, and the

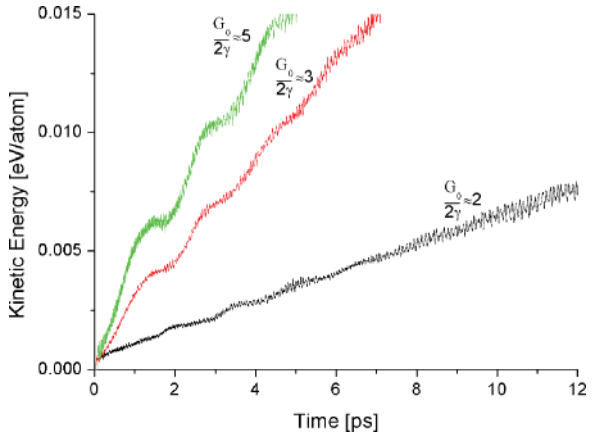

FIG. 11. (Color online) The instantaneous average kinetic energy per atom vs time in the (110)[1$\bar{1}$0] system for increased $\mathcal{G}_0$.

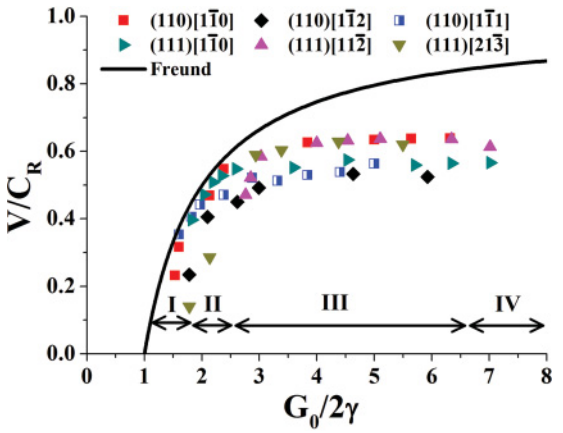

FIG. 12. (Color online) The normalized crack tip speed, V/C_{R}, vs the normalized $\mathcal{G}_0/2\gamma_s$ for the six cleavage systems of silicon. The full black line presents the Freund equation of motion.

results are shown in Fig. 14. The linear trend line shows that the strain energy inserted into the specimen was converted into surface energy and kinetic energy, and thus eliminated the existence of any other potential energy dissipation mechanism.

The variations of the phonon ERR, G_{ph}, with crack speed for six cleavage systems of silicon are shown in Fig. 15. Several features are evident from this relationship: $\mathcal{G}_{\text{ph}}$ at $V < 0.4C_{\text{R}}$ is small with negligible anisotropy but becomes a significant energy dissipation mechanism at $V > 0.5C_{\text{R}}$ with significant crystal anisotropy. $\mathcal{G}_{\text{ph}}$ prevents the crack from attaining C_{R}, as the terminal speed bounds between $0.52C_{\text{R}}$ and $0.64C_{\text{R}}$. At $V > 0.4C_{\text{R}}$, cracks on the (111) cleavage plane prefer to propagate in the [11$\bar{2}$] and [21$\bar{3}$] directions over the [1$\bar{1}$0] direction, whereas those on the (110) cleavage plane prefer the [1$\bar{1}$0] direction over the [11$\bar{1}$] and the [1$\bar{1}$2] directions.

D. Volume and temperature effect

We next calculated the terminal crack speed for different volumes of the cracked bodies. Samples with same geometry and boundary conditions, with heights, H, of 18, 55, 175,

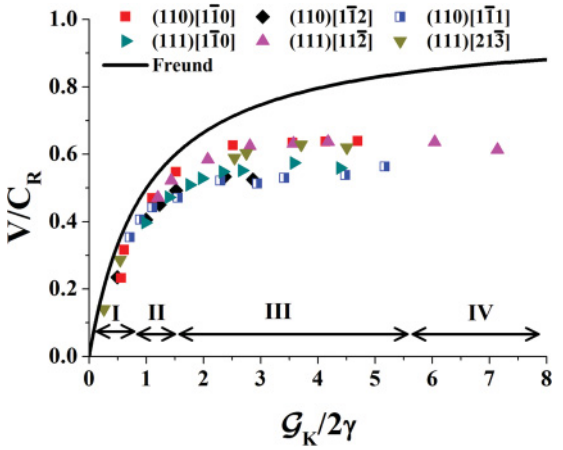

FIG. 13. (Color online) The normalized crack tip speed, V/C_{R}, with normalized kinetic ERR, $\mathcal{G}_{\text{K}}^{\text{MD}}/2\gamma_s$, for the six cleavage systems of silicon. The black line presents the Freund equation of motion.

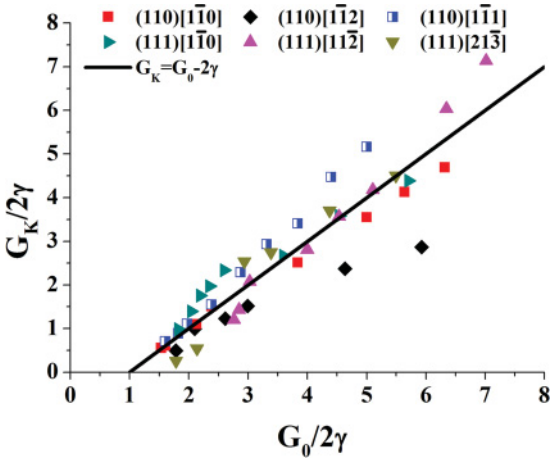

FIG. 14. (Color online) Variations of the normalized kinetic ERR, $\mathcal{G}_K^{MD}/2\gamma_s$, with the normalized strain ERR, $\mathcal{G}_0/2\gamma_s$. This relationship suggests that no other energy dissipation mechanisms exist during crack propagation in silicon.

553 nm, which contained 25 000, 250 000, 2.5 million, and 25 million atoms, respectively, were analyzed. The normalized terminal crack speeds, V_{max}/C_R, vs the specimens' height are shown in Fig. 16.

It is evident that as the volume of the cracked body decreases, the maximum crack speed decreases. For the 18-nm height specimen, maximum crack speed was $0.58C_R$. The MD with semi-empirical interatomic potential failed to evaluate crack speed above $0.65C_R$ in the largest volume and nonlinear deformations prevailed. The full circles in Fig. 16 denote the estimated results for physical experiments.

We repeated the computer "experiments" for crack propagation on the (110)[1$\bar{1}$0] cleavage system with initial specimen temperatures of 10K, 100K, and 300K. The terminal crack speed was plotted for different initial temperatures, as shown in Fig. 17. The results showed that the terminal steady state

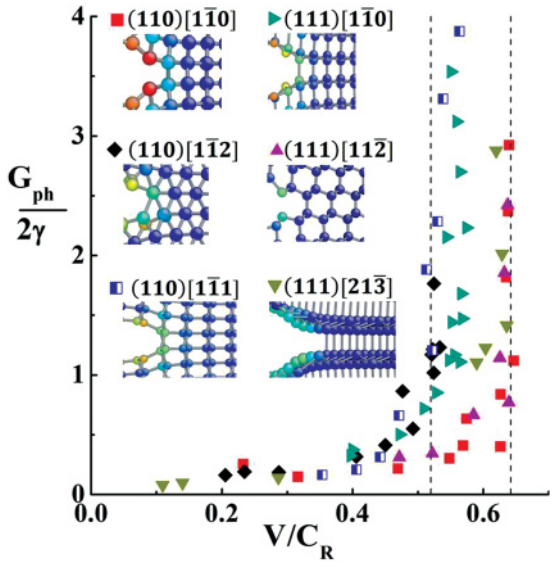

FIG. 15. (Color online) The normalized phonon ERR, $\mathcal{G}_{ph}/2\gamma_s$, vs the normalized crack speed, V/C_R, for the six different cleavage systems of silicon crystal.

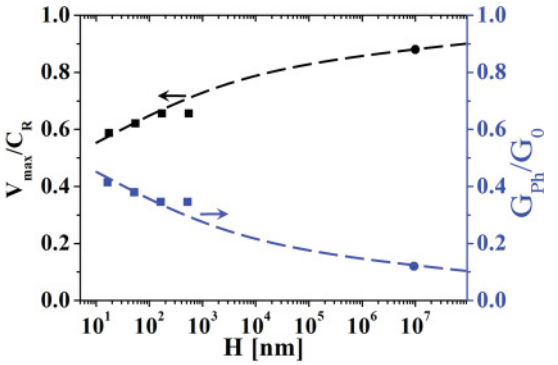

FIG. 16. (Color online) The maximum normalized crack speed vs specimen height, H, corresponds to higher specimen volume and relative phonon energy with respect to strain ERR (black and blue/medium gray full squares) and that estimated for experimental results (black and blue/medium gray full circles).

crack speed is almost not affected (within the crack detection error range) by the increased temperature (similar results were reported by Holland and Marder[27]), meaning that phonon emission ERR causes the reduced terminal speed irrespective of the temperature range of 10K–300K. Additionally, we performed our calculations at 10K to minimize the signal to noise ratio of phonon emission energy. Performing the same calculations at a higher temperature is possible but will raise numerical and physical problems that will complicate the data analysis process.

V. DISCUSSION

A. Dynamic fracture computer experiments

To perform dynamic fracture atomistic computer "experiments" one should make a number of decisions (e.g., simulation method, boundary conditions, and details of the loading scheme). The nonexistence of software that includes all the detailed capabilities to perform computer experiments and the high cost of the needed hardware make the attempt to include all the "experimental" details of crack dynamics almost impossible. Therefore, to justify the results obtained

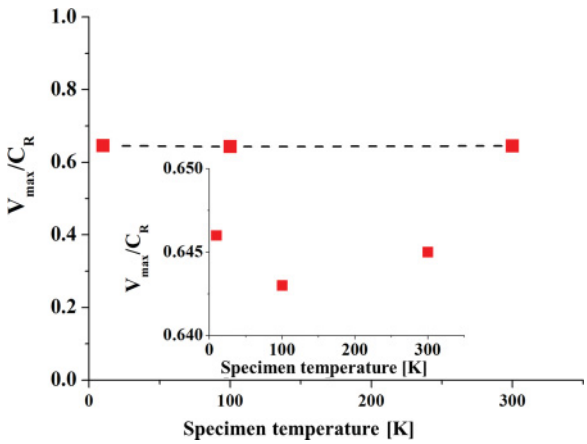

FIG. 17. (Color online) Variations of the terminal crack speed with specimen initial temperature. The crack propagation takes place on the (110)[1$\bar{1}$0] cleavage system.

by our computer experiments, we explain and rationalize each step of the experiment and discuss any ambiguous result.

1. The computational tool

In this investigation, we choose to use classical MD simulation as the main computational tool. The choice of the MD approach rather than other discrete lattice models was motivated by the request to use a simulation method that could cover the full spatial and temporal phononic spectrum. To date, there is no interatomic potential able to predict simultaneously the elastic, thermal, and brittle behavior of silicon crystal. Therefore, by choosing MD to model dynamic fracture, we renounce in advance the search for the absolute "truth" of the fracture dynamic process, and we limit ourselves to search for trends and phenomena that may be concluded from the MD calculations. We are aware that recent developments in the field of multiscale modeling intend to supply computational tools aimed at providing better properties of silicon. However, despite the recent achievements (e.g., Ref. 26), the software is still under development and the time needed to perform the calculations with the available computer power is still impractical.

2. The loading scheme

In this investigation, we decided to follow the loading scheme suggested by Gumbsch *et al.*,[15] with modifications. This method is combined from two main stages: a quasi-static and a dynamic loading. The former step was not taken by several authors investigating dynamic fracture (e.g., Refs. 14, 20, and 27). However, while performing preliminary computer experiments (not reported here), in which the quasi-static loading stage was omitted, we noticed the introduction of an artificial undesired shock wave into the specimen, mainly due to too high loading rates.

To allow calculations in a wide range of crack speeds, we used stepwise loading and homogeneous rescaling, which was applied instantaneously between two MD steps. It instantaneously changes the load level without creating any shock waves that may disturb the crack elastic fields. While changing the atomic displacements, the overall shape of the elastic strain field is maintained. Such rescaling of the displacements can be, in principle, used any time during a MD run to either increase or decrease the load level.[15]

3. The boundary conditions

Because the computer power available to us was limited, only small systems compared with the size of physical specimens were analyzed. The size limitation is usually solved by performing certain approximations that can be achieved by applying special boundary conditions (BC). For example, infinite specimen thickness (resulting from plain strain conditions along the crack front) is achieved by applying periodic BC on the large surfaces of the problem, which reduces, significantly, the number of atoms required in the computer specimen.

Phonons of a variety of amplitudes (e.g., elastic and thermal) are emitted out of the crack tip during crack dynamics; these phonons propagate in the specimen volume and interact with its boundaries, and some part of these phonons are reflected back toward the moving crack tip and may affect the fracture dynamics. In the field of wave mechanics, this problem is usually solved by applying absorbing BC (e.g., Ref. 28). Several absorbing methods were suggested to avoid phonon reflections at boundaries during fracture dynamics in a strip-like specimen (e.g., Ref. 15). The absorbing BC methods involve fictitious forces applied to boundary atoms or the use of non-Newtonian mechanics in some regimes of the specimen that may complicate any attempt to distinguish between the energy of elastic waves and thermal phonons. It also may increase the signal to noise ratio of the phonon emission energy release rate due to kinetic energy loss during fracture dynamics, caused by the absorbing BC. In this research, we calculated average crack velocity and average kinetic ERR based on fracture dynamics on a time interval that is shorter than that needed for interaction between the crack tip and reflected waves from the boundaries. Moreover, the loading scheme used in this research minimizes the amount of shock waves that may intensify this interaction.

4. The fracture dynamics

The exact scenario of bond ruptures and relaxation events requires a simulation method with quantum resolution near the crack tip. Because MD can only capture events at the atomistic scale, the discussion of the exact events that lead to bond rupture and phonon emission is redundant. Visualizations of fractured surfaces during crack propagation showed that they were atomically flat at intermediate driving force (regimes I–III in Fig. 12), which indicate that all the bond-rupture events are almost identical and that the modeled material is ideally brittle. On the other hand, the limitation of MD calculations to predict precise fracture dynamics is evident in regimes I and IV: due to the velocity gap phenomenon in the former and due to the inability of the interatomic potential to predict the brittle behavior at high strain levels in the latter. Overcoming this inaccessibility of MD may be achieved by suggesting improved interatomic potentials that will predict brittle behavior in high strains and by modifying the BC along the crack front. Because the solution of these shortcomings is yet unavailable, we deduced the conclusions based on fracture dynamics of the intermediate loading regimes (regime II and III in Fig. 12). These zones supplied most of the required information to point out the role played by phonon emission ERR in dynamic fracture.

B. Energy calculations with the strip-like specimen

In the following discussion, motivations, justifications, and implications of using Eq. (9) in the strip-like specimen are presented. Additionally, the justification of the combined continuum-based approach and atomistic computer calculations to evaluate the physical property $\mathcal{G}_{\mathrm{ph}}$ in the boundary value problem (BVP) is explained. Three different approaches of calculating $\mathcal{G}_{\mathrm{ph}}$ can be considered: extracting $\mathcal{G}_{\mathrm{ph}}$ directly (i) from atomic positions and velocities, (ii) from changes in the local stress field at the vicinity of the crack tip during fracture dynamics, and (iii) on the basis of variations in energy balance during fracture dynamics. Extracting $\mathcal{G}_{\mathrm{ph}}$ directly from atomic positions and velocities would require the development of computational tools that are able to distinguish between

elastic and nonelastic or thermal phonons emitted from the crack tip. This mission is complex mainly because of short times available for calculations and the anisotropic nature of the modeled material. The virial stress procedure usually employed to evaluate stress in atomistic calculations contains an atomic velocity–dependent term, which becomes significant in the vicinity of the crack tip, where atomic velocities are relatively high compared with bulk atomic velocities. Moreover, virial stress is an ensemble property that must be averaged over relatively long time and volume; that is, validity of the current definitions of stress during crack dynamics is dubious.

The lack of direct or stress-based methods for calculation of thermal phonon ERR imposed employing a method based on variations in energy balance during fracture dynamics. To separate between $\mathcal{G}_{\rm ph}$ and $\mathcal{G}_{\rm K}^{\rm MD}$, one should estimate the ERR of elastic waves, directly, from computer atomistic simulation, or theoretically, from the Freund equation of motion based on continuum mechanics approach ($\mathcal{G}_{\rm K}^{\rm F}$). Direct differentiation between lattice vibrations caused by elastic waves and nonelastic waves (thermal phonon) is difficult in our specimen and needs theoretical and computational tools currently unavailable. A theoretical estimate of the kinetic ERR of elastic waves can be made either by the Freund equation of motion for the crack propagation stage that doesn't include reflected waves or by other analytical solutions that consider possible effects of reflected waves.

Therefore, before estimating $\mathcal{G}_{\rm K}^{\rm F}$ by the Freund equation of motion, it is necessary to show that our computer "experiments" meet the conditions and assumptions that led to this equation. The Freund equation was developed for infinite elastic bodies, and it is valid only before interactions between elastic waves and specimen boundaries take place. It is assured in our calculations that elastic waves didn't reach the top and the bottom boundaries during, approximately, the first 4 ps of crack propagation. With this, we concluded that the Freund equation of motion is valid for the strip geometry with prescribed displacement boundary conditions. Furthermore, we claim that the elastic energy release rate, expressed by the dynamical universal function, is a general solution for dynamic crack propagation, as long as no stress waves are reflected from the boundaries. Indeed, $\mathcal{G}_{\rm K}^{\rm MD}$ for the six analyzed crack systems, shown in Fig. 13, agrees well with the Freund solution for the low-energy regime (stages I and II) and deviates only when $\mathcal{G}_{\rm ph}$ becomes significant.

C. Energy distribution in silicon crystals

Four regimes of $\mathcal{G}_0/2\gamma_s$ can be identified (Fig. 12). At low-strain ERR, marked by regime I in Fig. 12, a velocity gap of 0.2, 0.3, and 0.35 $C_{\rm R}$ was observed in the (110)[$1\bar{1}0$], (111)[$11\bar{2}$], and (111)[$1\bar{1}0$] crack systems, respectively. Only the crack system (110)[$1\bar{1}2$] showed a crack velocity as low as $0.05C_{\rm R}$. In regime II, the crack velocity varies as expected according to continuum mechanics based on the Freund equation of motion (solid line in Fig. 12). In this loading regime, the majority of the radiated waves are long elastic waves. Deviation from the continuum mechanic–based Freund equation of motion starts at regime III. The number of short waves emitted from the crack's tip increases with the applied strain energy release rate, thus dissipating a considerable amount of energy in the form of short waves not taken into account in the original Freund equation of motion, Eq. (1). In loading regime IV, surface features (e.g., branching and deflection) begin to emerge. Since experimentally the fracture surface of a single crystal such as silicon is atomically flat at high velocities,[19,21] this regime is neglected, and the calculations were terminated there. The same four different regimes can be indentified in Fig. 13 for kinetic energy.

D. The role of phonon emission in dynamic fracture

Based on the results presented in this investigation, we conclude that crack dynamics is governed by the crystallography of the cleavage system; hence, the phonon emission ERR is anisotropic. That is, the amount of energy dissipated by phonon emission varies with the cleavage system. We attribute this behavior to a local atomistic arrangement near the crack tip and to the anisotropic thermal properties of the model material.

The anisotropic nature of the phonon emission ERR has practical application. Consider a crack that propagates on cleavage system A with increasing speed. The crack is driven by energy considerations. When the kinetics of the crack propagation process leads the crack path to intersect with another cleavage system B, which dissipates less energy by phonon emission at certain crack speed, the crack will choose the path with the minimum energy; that is, the crack will deflect from cleavage system A to cleavage system B. Based on this physical argument, we demonstrated, in a previous publication,[29] several possible crack deflection mechanisms. The predicted transitions show the existence of preferred propagation directions on the (110) and (111) cleavage planes; that is, we predicted that the cracks propagating on the (110) cleavage plane will prefer the [$1\bar{1}0$] propagation direction over the [$11\bar{2}$] and [$1\bar{1}1$] propagation directions, whereas cracks propagating on the (111) cleavage plane prefer propagation in the [$21\bar{3}$] over the [$11\bar{2}$] and [110] propagation directions. Note that based on these results only, a preliminary and general conclusion can be drawn: cracks propagating on the (110) cleavage plane prefer the low-index direction (propagation in the [001] direction is excluded for being a unique direction), whereas cracks propagating on the (111) plane prefer the high-index direction.

VI. SUMMARY

We presented, in detail, a combined continuum mechanics approach and MD computer calculations method to evaluate anisotropic-, velocity-, and size-dependent phonon ERR as an energy dissipation mechanism occurring during dynamic crack propagation in brittle crystals. The motivations, justifications, and implications for using this method were thoroughly discussed. It was shown that the phonon emission energy release rate strongly depends on crack speed and the particular atomistic arrangement at the crack tip, and that its influence depends on specimen size. On the other hand, this ERR does not change at a temperature range of 10K–300K.

ACKNOWLEDGMENT

We gratefully acknowledge the financial support of the EU-FP-NMP grant "ADGLASS."

*Corresponding author: dsherman@tx.technion.ac.il

[1]L. Freund, *Dynamic Fracture Mechanics* (Cambridge Univ. Press, Cambridge, 1998).
[2]A. Stroh, Adv. Phys. **6**, 418 (1957).
[3]R. Weichert and K. Schönert, Int. J. Fract. **5**, 353 (1969).
[4]K. Fuller, P. Fox, and J. Field, Proc. R. Soc. London A **341**, 537 (1975).
[5]R. Weichert and K. Schönert, J. Mech. Phys. Solids **22**, 127 (1974).
[6]R. Weichert and K. Schönert, J. Mech. Phys. Solids **26**, 151 (1978).
[7]W. Döll, Eng. Fract. Mech. **5**, 259 (1973).
[8]J. R. Rice and N. Levy, in *Physics of Strength and Plasticity*, edited by A. S. Argon (The MIT Press, Cambridge, 1969), pp. 277–293.
[9]S. N. Atluri, M. Nakagak, T. Nishioka, and Z.-B. Kuang, Eng. Fract. Mech. **23**, 167 (1986).
[10]Z. B. Kuang and S. N. Atluri, J. Appl. Mech. **52**, 274 (1985).
[11]N. Sun and T. Hsu, Int. J. Fract. **78**, 67 (1996).
[12]C. Zhang and B. Karihaloo, Eng. Fract. Mech. **46**, 1023 (1993).
[13]J. Hauch, D. Holland, M. P. Marder, and H. L. Swinney, Phys. Rev. Lett. **82**, 3823 (1999).
[14]D. Holland and M. Marder, Phys. Rev. Lett. **80**, 746 (1998).
[15]P. Gumbsch, S. J. Zhou, and B. L. Holian, Phys. Rev. B **55**, 3445 (1997).
[16]D. Sherman, J. Mech. Phys. Solids **53**, 2742 (2005).
[17]D. Sherman and I. Be'ery, Scr. Mater. **49**, 551 (2003).
[18]D. Sherman and I. Be'ery, J. Mater. Res. **18**, 2379 (2003).
[19]D. Sherman and I. Be'ery, J. Mech. Phys. Solids **52**, 1743 (2004).
[20]J. G. Swadener, M. I. Baskes, and M. Nastasi, Phys. Rev. Lett. **89**, 085503 (2002).
[21]D. Sherman, M. Markovitz, and O. Barkai, J. Mech. Phys. Solids **56**, 376 (2008).
[22]Z. Jin, H. Gao, and P. Gumbsch, Phys. Rev. B **77**, 094303 (2008).
[23]J. Roth, F. Gahler, and H. Trebin, Int. J. Mod. Phys. C Phys. Comput. **11**, 317 (2000).
[24]D. Holland and M. Marder, Phys. Rev. Lett. **81**, 4029 (1998).
[25]J. Hutchinson and Z. Suo, Adv. Appl. Mech. **29**, 63 (1992).
[26]J. R. Kermode, T. Albaret, D. Sherman, N. Bernstein, P. Gumbsch, M. C. Payne, G. Csányi, and A. De Vita, Nature **455**, 1224 (2008).
[27]D. Holland and M. Marder, Adv. Mater. **11**, 793 (1999).
[28]D. Givoli, J. Comput. Phys. **94**, 1 (1991).
[29]F. Atrash, A. Hashibon, P. Gumbsch, and D. Sherman, Phys. Rev. Lett. **106**, 085502 (2011).